Biochemical and Biophysical Research Communications 533 (2020) 467–473

Contents lists available at ScienceDirect

Biochemical and Biophysical Research Communications

journal homepage: www.elsevier.com/locate/ybbrc

Andrographolide and its fluorescent derivative inhibit the main proteases of 2019-nCoV and SARS-CoV through covalent linkage

Tzu-Hau Shi [a, b], Yi-Long Huang [c], Chiao-Che Chen [a], Wen-Chieh Pi [d], Yu-Ling Hsu [e], Lee-Chiang Lo [e], Wei-Yi Chen [d], Shu-Ling Fu [f, **], Chao-Hsiung Lin [a, c, g, *]

[a] Department of Life Sciences and Institute of Genome Sciences, National Yang-Ming University, Taipei, 112, Taiwan
[b] Biomedical Industry Ph.D. Program, National Yang-Ming University, Taipei, 112, Taiwan
[c] Aging and Health Research Center, National Yang-Ming University, Taipei, 112, Taiwan
[d] Institute of Biochemistry and Molecular Biology, National Yang-Ming University, Taipei, 112, Taiwan
[e] Department of Chemistry, National Taiwan University, Taipei, 106, Taiwan
[f] Institute of Traditional Medicine, National Yang-Ming University, Taipei, 112, Taiwan
[g] Institute of Biopharmaceutical Sciences, National Yang-Ming University, Taipei, 112, Taiwan

ARTICLE INFO

Article history:
Received 16 August 2020
Accepted 22 August 2020
Available online 25 August 2020

Keywords:
2019-nCoV
SARS-CoV
Main protease
Andrographolide

ABSTRACT

The coronavirus disease 2019 (COVID-19) pandemic caused by 2019 novel coronavirus (2019-nCoV) has been a crisis of global health, whereas the effective vaccines against 2019-nCoV are still under development. Alternatively, utilization of old drugs or available medicine that can suppress the viral activity or replication may provide an urgent solution to suppress the rapid spread of 2019-nCoV. Andrographolide is a highly abundant natural product of the medicinal plant, *Andrographis paniculata*, which has been clinically used for inflammatory diseases and anti-viral therapy. We herein demonstrate that both andrographolide and its fluorescent derivative, the nitrobenzoxadiazole-conjugated andrographolide (Andro- NBD), suppressed the main protease (M^{pro}) activities of 2019-nCoV and severe acute respiratory syndrome coronavirus (SARS-CoV). Moreover, Andro-NBD was shown to covalently link its fluorescence to these proteases. Further mass spectrometry (MS) analysis suggests that andrographolide formed a covalent bond with the active site Cys^{145} of either 2019-nCoV M^{pro} or SARS-CoV M^{pro}. Consistently, molecular modeling analysis supported the docking of andrographolide within the catalytic pockets of both viral M^{pro}s. Considering that andrographolide is used in clinical practice with acceptable safety and its diverse pharmacological activities that could be beneficial for attenuating COVID-19 symptoms, extensive investigation of andrographolide on the suppression of 2019-nCoV as well as its application in COVID-19 therapy is suggested.

1. Introduction

The outbreak of COVID-19, caused by a 2019-nCoV, is an urgent global health crisis which requires a timely solution. As end of July 2020, there are approximately eighteen million confirmed cases and seven hundred thousand deaths worldwide. Currently, the target-based therapeutics and effective treatment regimens for COVID-19 are still limited. One of the potential strategies is to target the proteins which are essential for life cycle of 2019-nCoV, such as main protease (M^{pro}) and papain-like protease (PL^{pro}) [1]. M^{pro} is the viral protease involved in production of functional polyproteins required for viral replication, and no human homolog of this protein exists [2]. Remarkably, protein sequence of 2019-nCoV M^{pro} is highly similar to that of the SARS-CoV M^{pro} which is a proven target for reducing viral load of SARS [2,3]. Therefore, 2019-nCoV M^{pro} is a promising target for therapeutic intervention against COVID-19. Indeed, *in vitro* and *in silico* studies on identifying potential M^{pro} inhibitors are rapidly growing in numbers [3–5]. Moreover, lopinavir/ritonavir, previously identified as HIV protease inhibitors and found to exhibit anti-SARS-CoV activity *in vitro* and *in clinical*, have been proposed to bind 2019-nCoV M^{pro} and are being investigated for COVID-19 treatments [6,7]. However, several clinical trials indicate that they have limited efficacy in treating COVID-19 and

* Corresponding author. Department of Life Sciences and Institute of Genome Sciences, National Yang-Ming University, Taipei, 112, Taiwan.
** Corresponding author.
E-mail addresses: slfu@ym.edu.tw (S.-L. Fu), chlin2@ym.edu.tw (C.-H. Lin).

https://doi.org/10.1016/j.bbrc.2020.08.086
0006-291X/

caused significant adverse effects, such as gastrointestinal intolerance and hepatotoxicity [8].

Recently, a three-dimensional (3D) structure of 2019-nCoV M^{pro} including the substrate-binding pocket has been illustrated [4]. In addition, M^{pro} in SARS-CoV or 2019-nCoV is classified as a cysteine protease which involves an active site cysteine in its catalytic dyad. It has been shown that M^{pro} could be inactivated by the inhibitors initiating a Michael addition reaction on the active site cysteine [2,4]. Therefore, the Michael acceptor-containing compounds which can fit in the catalytic pocket of 2019-nCoV M^{pro} may serve as attractive drug candidates for treating COVID-19.

Plant-derived natural products play crucial roles in new drug development [9]. Andrographolide, a lactone diterpenoid compound highly abundant in leaves of medicinal plant *Andrographis paniculata*, has been demonstrated to exhibit diverse pharmacological activities, including anti-inflammatory, anti-viral, anti-cancer and hepatoprotective effects [10]. Both *A. paniculata* extract and andrographolide alone are currently used worldwide for treating upper respiratory diseases as well as inflammatory diseases [10–12]. In addition, their clinical trials demonstrate that no significant adverse effects were observed in patients [10–12]. More importantly, andrographolide which contains a Michael acceptor group has been shown to react with the Cys^{62} of NF-κB-p50 through covalent linkage [13,14], rendering it as a potential inhibitor of 2019-nCoV M^{pro}. In this study, we investigated the inhibitory effects of andrographolide and its fluorescent derivative on the *in vitro* activity of 2019-nCoV M^{pro}.

2. Material and methods

2.1. Chemicals and reagents

Andrographolide and disulfiram were purchased from Sigma-Aldrich (USA). Chemical syntheses of ANDRO-NBD and NCTU-048 were performed based on our previous studies [15,16]. Sequencing grade chymotrypsin was obtained from Promega (USA).

2.2. Protein expression and purification of SARS-CoV M^{pro} and 2019-nCoV M^{pro}

Preparation of the recombinant SARS-CoV M^{pro} was performed following a previous report [17]. Moreover, the DNA sequence of 2019-nCoV M^{pro} was cloned into a pET-29a vector to encode recombinant protease with a C-terminal His_6-tag. Upon plasmid transformation and IPTG induction in BL21 *E. coli* strain, the collected lysate supernatant was further purified by Ni-NTA affinity column (Qiagen, Germany) and S-100 size-exclusion chromatography column (GE Healthcare, USA) to produce pure 2019-nCoV M^{pro}.

2.3. Protease activity assay

Activities of 2019-nCoV M^{pro} and SARS-CoV M^{pro} were measured following a previous cleavage assay which used a fluorogenic peptide substrate (Abz-TSAVLQSGFRK-Dnp) in phosphate buffered saline (PBS) buffer (20 mM, pH 7.6) at 30 °C for 3 min as [18]. Upon the cleavage by protease, the quencher dinitrophenyl (Dnp) at C-terminal was released from the N-terminal fluorophore aminobenzoyl (Abz). Subsequently, the fluorescence at 423 nm was detected with excitation at 321 nm using a PerkinElmer LS 50B luminescence spectrometer (UK). The reaction concentrations of peptide substrate were ranged from 2 μM to 40 μM in PBS buffer (20 mM, pH 7.6), whereas the concentration of 2019-nCoV M^{pro} and SARS-CoV M^{pro} were respectively kept as 0.12 μM and 0.48 μM. Kinetics parameters like K_m and k_{cat} were determined by fitting the initial velocities at different substrate concentrations to a Michaelis-Menten equation, as described previously [18].

2.4. Inhibition of M^{pro} activity and determination of the half-maximal inhibitory concentration (IC_{50})

To determine inhibition of M^{pro} activity, inhibitor (0 μM–20 μM) and fluorogenic peptide substrate (5 μM) in PBS buffer (20 mM, pH 7.6) were first equilibrated at 30 °C for 3 min, followed by addition of protease (0.12 μM 2019-nCoV M^{pro} or 0.48 μM SARS-CoV M^{pro}) and further incubation at 30 °C for 3 min. As described above, enzymatic activity was determined and the measured velocities at different inhibitor concentrations were fitted to obtain IC_{50} according to the following equation:

$$v = \frac{v_0}{(1 + IC_{50}^n)/[I]^n}$$

in which v is the velocity with incubation of inhibitor at different concentration [I] and the v_0 is the initial velocity without incubation of inhibitor, while *n* is the Hill constant.

2.5. Fluorescence detection of main proteases upon inhibition with Andro-NBD

A total of 3 μM M^{pro} was treated with Andro-NBD in various molar ratios at 25 °C for 1 h and then analyzed by 12% SDS-PAGE. The resulting polyacrylamide gels were scanned for fluorescence at 520 nm under excitation at 488 nm using Amersham Imager 680 (GE healthcare, USA).

2.6. Docking analysis

The 3D structures of viral main protease were downloaded from the protein data bank (PDB, https://www.rcsb.org) which collects the published X-ray structures of SARS-CoV M^{pro} and 2019-nCoV M^{pro} [4,19]. Water molecules, ions, co-crystalized ligand were first removed from original structure prior to docking experiment, and chemical structure of andrographolide was added. The resulted complex of protein/andrographolide was subjected to molecular docking using Arguslab 4.0.1 to evaluate the putative ligand-binding site and release of free energy [20]. The optimal docking sites for ligand were accordingly predicted.

2.7. Statistical analysis

All of the data were represented as the mean ± standard derivation (SD) from three independent experiments. * represents p-value <0.05; ** represents p-value <0.01; *** represents p-value <0.001 by Student's *t*-test.

3. Results

3.1. 2019-nCoV M^{pro} and SARS-CoV M^{pro} shares similar consensus substrate sequence and enzyme kinetics

Recent genome analysis of 2019-nCoV revealed the organization of its open reading frame 1 (ORF1) which encodes two polyproteins consisting of all the non-structural proteins needed for virus replication and is very similar to SARS-CoV [21,22] (Fig. S1). In addition, sequence alignment of main proteases from 2019-nCoV, SARS-CoV and MERS-CoV showed that 2019-nCoV M^{pro} and SARS-CoV M^{pro} shares 96% identity, whereas the identity between 2019-nCoV M^{pro} and MERS-CoV M^{pro} is only 51% (Fig. S2). Because M^{pro} is the essential protease which is responsible to produce the

individual non-structural proteins upon proteolytic cleavage on the primary polyproteins, we further aligned amino acid sequences of all the 12 cleavage sites by 2019-nCoV M^{pro} (Fig. S3A). Among these sites, 8 of them are completely conserved between 2019-nCoV M^{pro} and SARS-CoV M^{pro}, including the peptide sequence between nsp4 and nsp5 (-TSITSAVLQSGFRKMAFP-) (Fig. S3B). Previously, a fluorogenic peptide (Abz-TSAVLQSGFRK-Dnp) which contains both a fluorophore (Abz) and its quencher (Dnp), has been used to determine the protease activity of SARS-CoV M^{pro} (Fig. S3C) [23]. Upon the cleavage of this peptide probe by protease, the fluorophore (Abz) was separated from its quencher and thus emitted fluorescence under UV excitation. We therefore prepared the recombinant 2019-nCoV M^{pro} and SARS-CoV M^{pro}, and measured their protease activities using this fluorogenic probe (Fig. 1A). Results of the protease activity assay revealed that 2019-nCoV M^{pro} exhibits higher activity and catalytic efficiency than SARS-CoV M^{pro} (Fig. 1B and Table 1).

3.2. Sedimentation coefficient distribution suggests a dimeric quaternary structure of 2019-nCoV M^{pro}

SARS-CoV M^{pro} was previously shown to function in a dimeric form. We therefore measured the continuous sedimentation coefficient distribution using analytical ultracentrifugation (AUC) to determine whether 2019-nCoV M^{pro} forms a homodimer (Fig. 1C). The profiles of quaternary structure at different concentrations suggest that 2019-nCoV M^{pro} exists predominantly in a dimeric structure (Fig. 1D), using SARS-CoV M^{pro} as a reference (Fig. 1E). In addition, SARS-CoV M^{pro} was previously shown to increase its monomeric form when existed in acidic environment [23]. However, further AUC experiments of 2019-nCoV M^{pro} under acidic condition (pH 6) only slightly increased its monomeric ratio. (Fig. S4).

3.3. Andrographolide inhibits protease activities of 2019-nCoV M^{pro} and SARS-CoV M^{pro}

Andrographolide has been reported to inhibit protein function through a Michael addition reaction with the free thiol side chain of cysteine [13,14]. We thus further examined whether the thiol-sensitive andrographolide could inhibit the cysteine proteases like 2019-nCoV M^{pro} and SARS-CoV M^{pro}. As shown in Fig. 2A, andrographolide inhibited protease activity of 2019-nCoV M^{pro} at IC_{50} of 15.05 ± 1.58 μM, whereas SARS-CoV M^{pro} was inhibited by andrographolide with an IC_{50} of 5.00 ± 0.67 μM. In addition, a previously reported fluorescent probe of andrographolide (Andro-

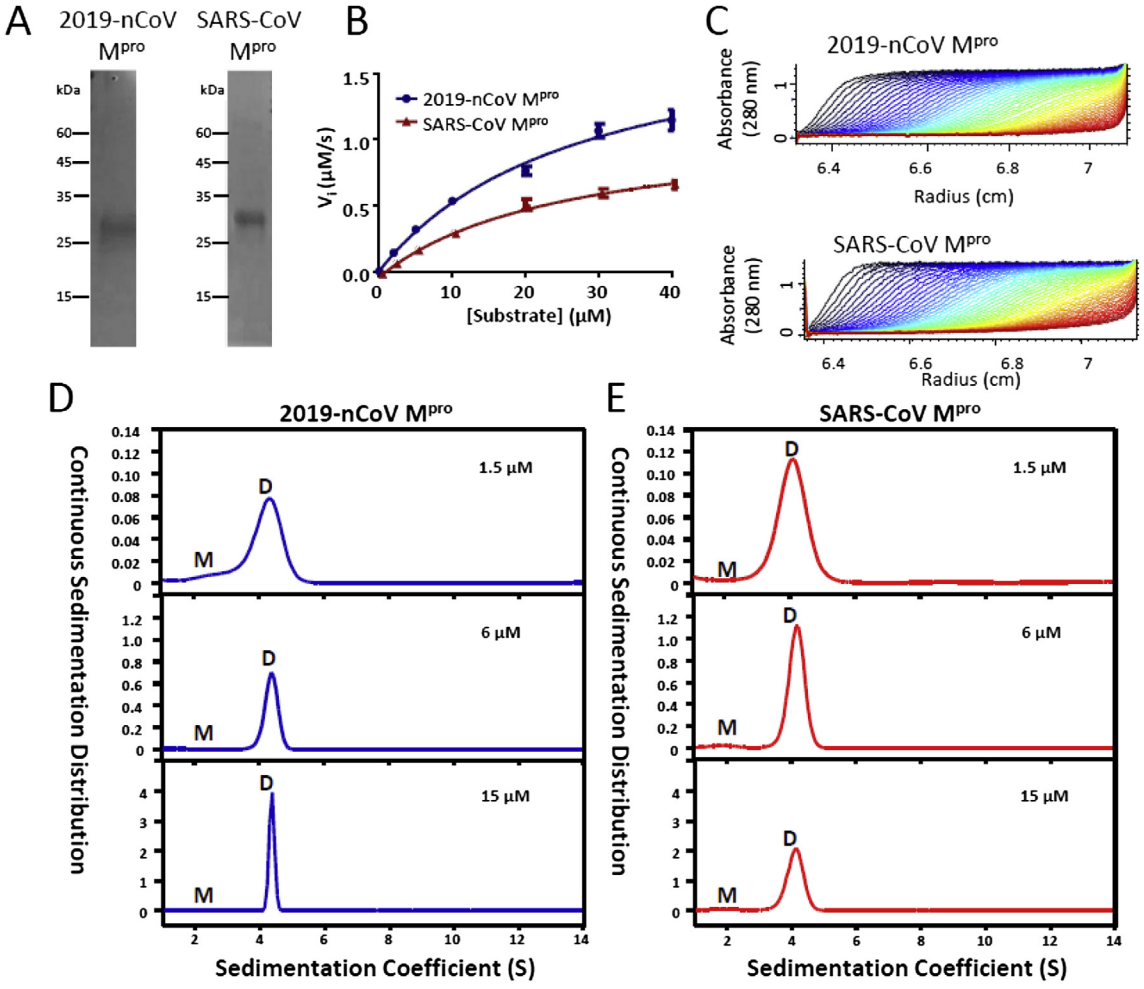

Fig. 1. Enzymatic activities and quaternary structure analyses of the 2019-nCoV M^{pro} and SARS-CoV M^{pro}. (A) Expression and purification of 2019-nCoV M^{pro} and SARS-CoV M^{pro}. (B) Enzyme activities of 2019-nCoV M^{pro} and SARS-CoV M^{pro} were measured using a proteolytic activity assay. (C) Absorbance patterns acquired during the sedimentation velocity experiment. (D) Profiles of 2019-nCoV M^{pro} quaternary structures at various protein concentration. M as monomer and D as Dimer. (E) Profiles of SARS-CoV M^{pro} quaternary structures at various protein concentration.

Table 1
Comparison of kinetics parameters and dimer dissociation constants.

Enzymes	Kinetics parameters[a]			Dimer dissociation constants K_d (μM)
	K_m (μM)	k_{cat} (s^{-1})	k_{cat}/K_m ($s^{-1}\mu M^{-1}$)	
2019-nCoV M^{pro}	27.56 ± 4.94	163.69 ± 15.09	5.94 ± 3.05	1.23
SARS-nCoV M^{pro}	25.83 ± 4.20	76.48 ± 6.04	2.96 ± 1.44	0.35

[a] All the experiments were performed in triplicates. K_m, Machaelis-Menten constant; k_{cat}, catalytic constant; k_{cat}/K_m, specificity constant for hydrolysis of peptide substrate. (Abz-TSAVLQSGFRK-Dnp).

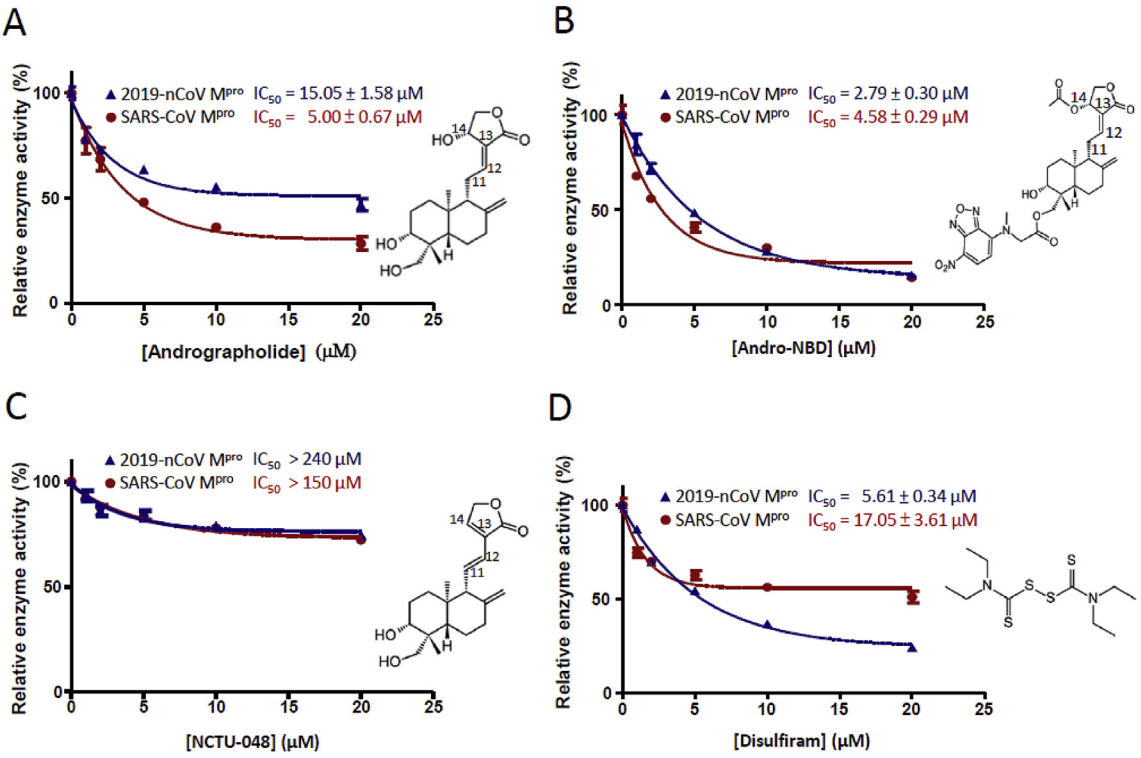

Fig. 2. Inhibition of 2019-nCoV M^{pro} activity by andrographolide and its derivatives. Protease activities of 2019-nCoV M^{pro} or SARS-CoV M^{pro} in the presence of inhibitors at five different concentrations was measured. IC_{50} of (A) andrographolide (B) Andro-NBD (C) NCTU-048 and (D) disulfiram were determined and shown respectively. All the experiments were independently carried out in triplicates.

NBD) also inhibited both 2019-nCoV M^{pro} and SARS-CoV M^{pro} at IC_{50} of 2.79 ± 0.30 μM and 4.58 ± 0.29 μM, respectively (Fig. 2B). To investigate whether andrographolide and Andro-NBD inhibited 2019-nCoV M^{pro} and SARS-CoV M^{pro} in a Michael addition-dependent manner, a thiol-insensitive andrographolide derivative (NCTU-048) was also examined in the protease activity assay and it exhibited relatively low protease inhibition (Fig. 2C). Moreover, a previously reported SARS-CoV M^{pro} inhibitor (disulfiram) was also investigated for its inhibition on 2019-nCoV M^{pro} and the result showed an IC_{50} of 5.61 ± 0.34 μM (Fig. 2D).

3.4. Andro-NBD and andrographolide form covalent linkages with 2019-nCoV M^{pro} and SARS-CoV M^{pro}

As described above, both andrographolide and Andro-NBD were shown to inhibit the activity of 2019-nCoV M^{pro}. We have previously demonstrated that Andro-NBD forms a covalent bond with p50 subunit of NF-kB [15]. Whether Andro-NBD also inhibits 2019-nCoV M^{pro} through a covalent linkage was herein investigated. As shown in Fig. 3A, protein bands of 2019-nCoV M^{pro} treated with Andro-NBD at different concentrations exhibited fluorescent signals on SDS-PAGE gels, whereas treatments of nitrobenzoxadiazole (NBD) alone or together with andrographolide did not induce such fluorescence. Similarly, Andro-NBD also formed a covalent linkage with SARS-CoV M^{pro} (Fig. S5). Furthermore, C145A mutation of 2019-nCoV M^{pro} abolished the above fluorescence by treatment of Andro-NBD at all concentrations (Fig. 3B). Moreover, the andrographolide-treated 2019-nCoV M^{pro} was subjected to mass spectrometry analysis for the evidence of covalent linkage. As shown in Fig. S6A, the peptide signal at 2328.0330 *m/z* matched to the 2019-nCoV M^{pro} residue (141–159) which is deduced to carry a dehydrated andrographolide (+332 Da) on Cys^{145}. Further MS/MS fragmentation analysis of such mass signal verified the partial amino acid sequences of this Cys^{145}-containing residue. Similarly, the andrographolide-labeled residues of SARS-CoV M^{pro} was also identified (Fig. S6B). Taken together, we have demonstrated that Andro-NBD and andrographolide form covalent linkages with 2019-nCoV M^{pro} and SARS-CoV M^{pro}.

3.5. Andrographolide can dock into the catalytic pockets of 2019-nCoV M^{pro} and SARS-CoV M^{pro}

We further carried out the docking experiment using Arguslab modeling program [20] to study whether andrographolide enters

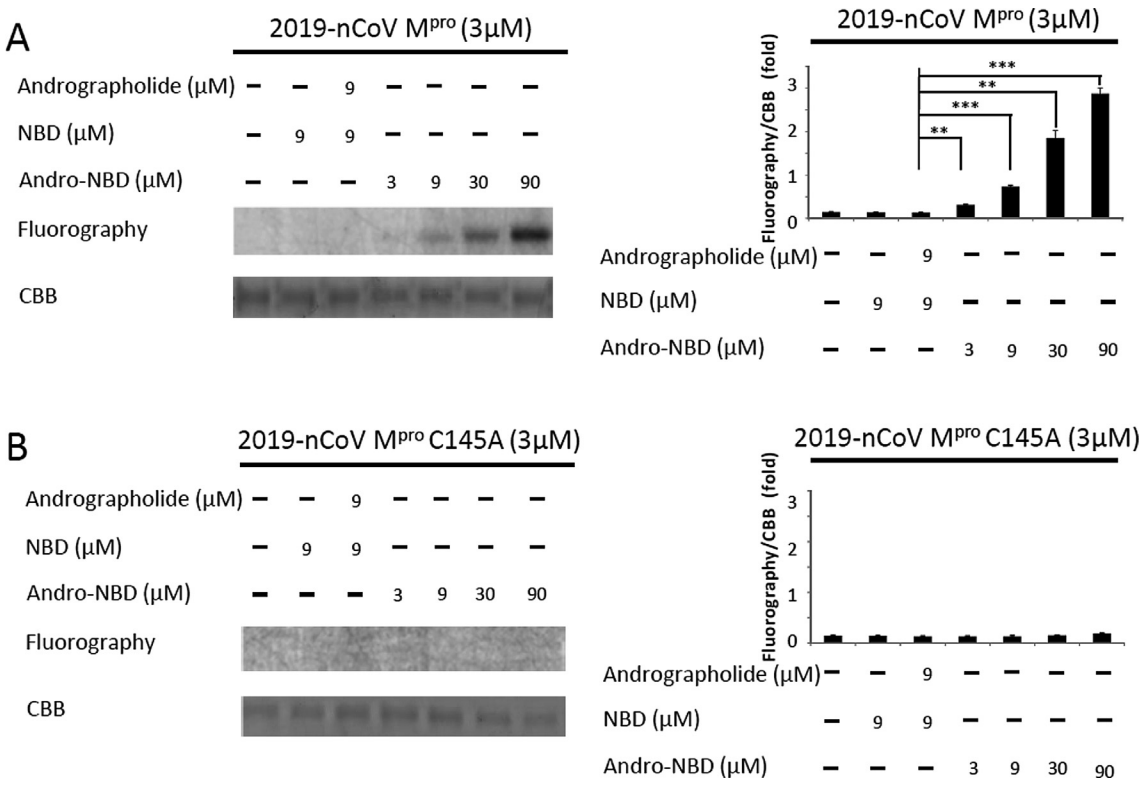

Fig. 3. Andro-NBD formed covalent linkage with Cys^{145} of 2019-nCoV M^{pro}. (A) 2019-nCoV M^{pro} was incubated with various concentration of Andro-NBD at 25 °C for 1 h and subsequently analyzed by SDS-PAGE. Gel fluorescence was detected and scanned for image. Quantitative data were shown as mean ± SD from three independent experiments. ** represents p-value <0.01 and *** represents p-value <0.001. (B) The C145A mutant 2019-nCoV M^{pro} was also incubated with various concentration of Andro-NBD at 25 °C for 1 h and subsequently analyzed by SDS-PAGE. No gel fluorescence was detected.

the catalytic pockets of 2019-nCoV M^{pro} (PDB 6LU7) and SARS-CoV M^{pro} (PDB 1UK4) [4,19]. As shown in Fig. 4A, modeling results suggested the presence of andrographolide in the catalytic pocket of 2019-nCoV M^{pro}. The binding affinity of andrographolide in 2019-nCoV M^{pro} was estimated to be −9.72 kcal/mol (ΔG) and the distance between Cys^{145} and the acceptor carbon of Michael reaction (C12 of andrographolide) is 3.7 Å (Fig. 4B and C). Similarly, SARS-CoV M^{pro} exhibits comparable binding affinity of andrographolide at −7.85 kcal/mol and its Cys^{145} is 4.8 Å away from Michael addition site (Fig. 4E and F). Together, these results support our findings of andrographolide-mediated inhibition and covalent linkage of 2019-nCoV M^{pro} and SARS-CoV M^{pro}.

4. Discussion

Our results demonstrated that andrographolide can inhibit the activity of 2019-nCoV M^{pro} (IC_{50} = 15.05 ± 1.58 μM; Fig. 2A). Molecular modeling data further support that andrographolide can enter the proposed substrate-binding pocket of 2019-nCoV M^{pro} (Fig. 4), such observation is consistent with a recent *in silico* study suggesting that andrographolide can dock in the binding site of 2019-nCoV M^{pro} [24]. Furthermore, we also found that Andro-NBD, but not compound 048, strongly inhibited the activity of 2019-nCoV M^{pro} (IC_{50} = 2.79 ± 0.3 μM for Andro-NBD; > 240 μM for NCTU-048) (Fig. 2). 2019-nCoV M^{pro} is a cysteine protease known to be inactivated by Michael acceptor inhibitor N3 [4]. Andrographolide belongs to the Michael acceptor category of electrophilic natural compounds and it has been reported to react with Cys62 of NF-κB-p50 at C12-13 exocyclic double bond to form a covalent adduct through a Michael addition [13,14]. Andro-NBD also can covalently bond to the p50, presumably through a similar mechanism [15]. On the other hand, the compound NCTU-048 with much weaker bioactivity than andrographolide is suggested to interact with NF-κB-p50 through different mechanism [25]. Accordingly, Andro-NBD was shown capable of forming covalent linkage with 2019-nCoV M^{pro}, whereas C145A mutation of protease abolished such covalent bond (Fig. 3). Furthermore, MS-based sequencing analysis suggested that andrographolide forms a covalent bond with active site Cys^{145} of 2019-nCoV M^{pro} (Fig. S6). Notably, such covalent linkage of andrographolide with reactive cysteine of protein target has also been reported previously [26]. Together, our data support a model that Andro and Andro-NBD could enter the substrate-binding pocket and initiate Michael reaction with 2019-nCoV M^{pro}, leading to the inactivation of protease activity.

Lopinavir/ritonavir, the HIV protease inhibitors previously identified with anti-SARS-CoV activity *in vitro* and in clinical, was proposed to bind 2019-nCoV M^{pro} and thus has been investigated for COVID-19 treatments [6,7]. Currently, inhibition of 2019-nCoV by Lopinavir/ritonavir has not been experimentally demonstrated. Data of several clinical trials indicate their roles in treating COVID-19 are limited and their significant adverse effects, such as gastrointestinal intolerance and hepatotoxicity, have been observed [8]. Disulfiram, an FDA-approved drug for treating alcohol addiction, has been reported to inhibit 2019-nCoV M^{pro} [4] but its clinical efficacy against COVID-19 remains to be determined. Therefore, development of 2019-nCoV M^{pro} inhibitors from clinically available medicine is still in great demand.

Andrographis paniculata along with its major ingredient, andrographolide, have been used as herbal medicine for treating anti-inflammatory diseases in Asia and in Europe [10]. Accumulating evidences from clinical studies indicate that *Andrographis paniculata* extract and andrographolide reduce symptoms in patients with HIV, upper respiratory infection, ulcerative colitis or rheumatoid arthritis with considerable safety [10,27–30].

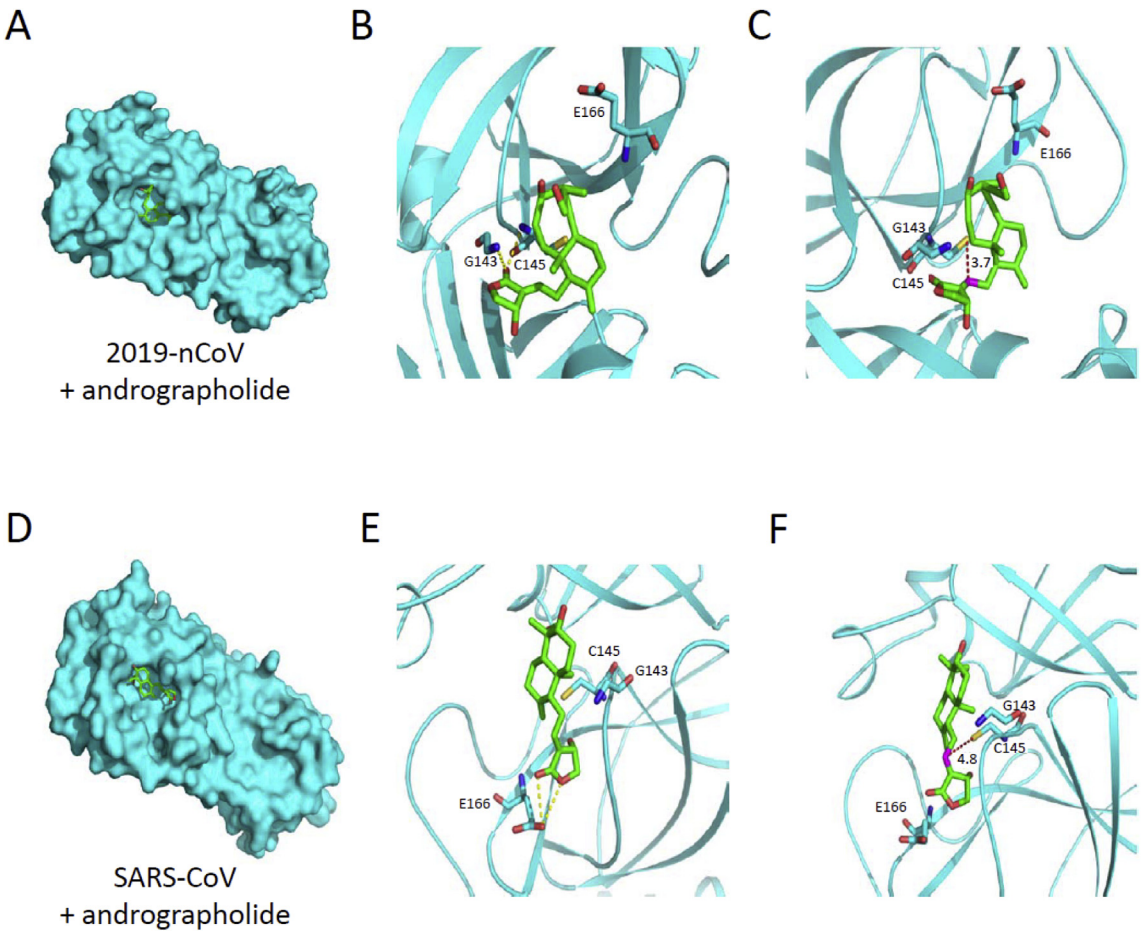

Fig. 4. Prediction of the putative binding site for andrographolide in 2019-nCoV M^{pro} and SARS-CoV M^{pro}. (A) Overall predicted surface model for the complex of 2019-nCoV M^{pro} (cyan) and andrographolide (green) was established. (B) Amplified region of catalytic pocket highlighting the hydrogen bonds (yellow dot line) between M^{pro} residues and andrographolide. (C) The distance (red dot line) between M^{pro} Cys^{145} (yellow) and Michael acceptor carbon (magenta) of andrographolide is shown. (D) Overall predicted surface model for the complex of SARS-CoV M^{pro} (cyan) and andrographolide (green) was established. (E, F) Amplified regions of catalytic pocket for complex in (D). (For interpretation of the references to colour in this figure legend, the reader is referred to the Web version of this article.)

Furthermore, experimental data from preclinical studies demonstrated the diverse pharmacological mechanisms of *A. paniculata* and andrographolide, including those in anti-inflammation, antiviral activity, hepatoprotection, anti-pulmonary fibrosis, and cardiopretection [10,12,31–33] Particularly, their safety profile in clinical uses are well accepted and andrographolide up to 30 μM did not cause cytotoxicity on human peripheral blood mononuclear cells (PBMC) [10,34].

In this study, we revealed that andrographolide and its derivative inhibits the activity of main protease and thus likely to impair the replication of SARS-CoV and 2019-nCoV. Considering that andrographolide is widely demonstrated in clinical application with acceptable safety and exhibits diverse pharmacological activities which could be beneficial for attenuating COVID-19 symptoms, application of andrographolide on COVID-19 therapy certainly merit further investigation.

Declaration of competing interest

The authors declare no conflicts of interest.

Acknowledgements

We specifically thank Dr. Chi-Yuan Chou from the Department of Life Sciences at National Yang-Ming University for providing the SARS-CoV M^{pro}, the fluorogenic peptide probe and the technical assistance of AUC. We also thank Dr. Chen-Chung Liao of Proteomics Research Center at National Yang-Ming University for the technical assistance of MS analysis and data processing.

Appendix A. Supplementary data

Supplementary data to this article can be found online at https://doi.org/10.1016/j.bbrc.2020.08.086.

Funding information

This work was supported by grants from the Ministry of Science and Technology in Taiwan (MOST 106-2320-B-010-006-MY3, MOST 106-2311-B-010-004-MY3 and MOST 109-2327-B-010-005, MOST 109-2321-B-010-003).

References

[1] G. Li, E. De Clercq, Therapeutic options for the 2019 novel coronavirus (2019-nCoV), Nat. Rev. Drug Discov. 19 (2020) 149–150.
[2] T. Pillaiyar, M. Manickam, V. Namasivayam, Y. Hayashi, S.H. Jung, An overview of severe acute respiratory syndrome-coronavirus (SARS-CoV) 3CL protease inhibitors: Peptidomimetics and small molecule chemotherapy, J. Med. Chem. 59 (2016) 6595–6628.
[3] J.S. Morse, T. Lalonde, S. Xu, W.R. Liu, Learning from the Past: Possible urgent prevention and treatment options for severe acute respiratory infections

caused by 2019-nCoV, Chembiochem 21 (2020) 730–738.
[4] Z. Jin, X. Du, Y. Xu, Y. Deng, M. Liu, Y. Zhao, B. Zhang, X. Li, L. Zhang, C. Peng, Y. Duan, J. Yu, L. Wang, K. Yang, F. Liu, R. Jiang, X. Yang, T. You, X. Liu, X. Yang, F. Bai, H. Liu, X. Liu, L.W. Guddat, W. Xu, G. Xiao, C. Qin, Z. Shi, H. Jiang, Z. Rao, H. Yang, Structure of M(pro) from COVID-19 virus and discovery of its inhibitors, Nature (2020).
[5] M.T. Ul Qamar, S.M. Alqahtani, M.A. Alamri, L.L. Chen, Structural basis of SARS-CoV-2 3CL(pro) and anti-COVID-19 drug discovery from medicinal plants, J Pharm Anal (2020).
[6] L. Dong, S. Hu, J. Gao, Discovering drugs to treat coronavirus disease 2019 (COVID-19), Drug Discov Ther 14 (2020) 58–60.
[7] B. Nutho, P. Mahalapbutr, K. Hengphasatporn, N.C. Pattaranggoon, N. Simanon, Y. Shigeta, S. Hannongbua, T. Rungrotmongkol, Why are lopinavir and ritonavir effective against the newly emerged coronavirus 2019? Atomistic insights into the inhibitory mechanisms, Biochemistry (2020).
[8] J.M. Sanders, M.L. Monogue, T.Z. Jodlowski, J.B. Cutrell, Pharmacologic treatments for coronavirus disease 2019 (COVID-19): a review, J. Am. Med. Assoc. (2020).
[9] D.J. Newman, G.M. Cragg, Natural products as sources of new drugs from 1981 to 2014, J. Nat. Prod. 79 (2016) 629–661.
[10] Y. Dai, S.R. Chen, L. Chai, J. Zhao, Y. Wang, Y. Wang, Overview of pharmacological activities of Andrographis paniculata and its major compound andrographolide, Crit. Rev. Food Sci. Nutr. 59 (2019) S17–S29.
[11] I. Jantan, W. Ahmad, S.N. Bukhari, Plant-derived immunomodulators: an insight on their preclinical evaluation and clinical trials, Front. Plant Sci. 6 (2015) 655.
[12] T. Jayakumar, C.Y. Hsieh, J.J. Lee, J.R. Sheu, Experimental and clinical pharmacology of Andrographis paniculata and its major bioactive phytoconstituent andrographolide, Evid Based Complement Alternat Med 2013 (2013) 846740.
[13] M. Gersch, J. Kreuzer, S.A. Sieber, Electrophilic natural products and their biological targets, Nat. Prod. Rep. 29 (2012) 659–682.
[14] Y.F. Xia, B.Q. Ye, Y.D. Li, J.G. Wang, X.J. He, X. Lin, X. Yao, D. Ma, A. Slungaard, R.P. Hebbel, N.S. Key, J.G. Geng, Andrographolide attenuates inflammation by inhibition of NF-kappa B activation through covalent modification of reduced cysteine 62 of p50, J. Immunol. 173 (2004) 4207–4217.
[15] Y.H. Hsu, Y.L. Hsu, S.H. Liu, H.C. Liao, P.X. Lee, C.H. Lin, L.C. Lo, S.L. Fu, Development of a bifunctional andrographolide-based chemical probe for pharmacological study, PloS One 11 (2016), e0152770.
[16] S.H. Liu, C.H. Lin, F.P. Liang, P.F. Chen, C.D. Kuo, M.M. Alam, B. Maiti, S.K. Hung, C.W. Chi, C.M. Sun, S.L. Fu, Andrographolide downregulates the v-Src and Bcr-Abl oncoproteins and induces Hsp90 cleavage in the ROS-dependent suppression of cancer malignancy, Biochem. Pharmacol. 87 (2014) 229–242.
[17] S.C. Cheng, G.G. Chang, C.Y. Chou, Mutation of Glu-166 blocks the substrate-induced dimerization of SARS coronavirus main protease, Biophys. J. 98 (2010) 1327–1336.
[18] P.Y. Lin, C.Y. Chou, H.C. Chang, W.C. Hsu, G.G. Chang, Correlation between dissociation and catalysis of SARS-CoV main protease, Arch. Biochem. Biophys. 472 (2008) 34–42.
[19] K. Anand, H. Yang, M. Yang, Y. Ding, Y. Liu, Z. Lou, Z. Zhou, L. Sun, L. Mo, S. Ye, H. Pang, G.F. Gao, M. Bartlam, R. Hilgenfeld, Z. Rao, The crystal structures of severe acute respiratory syndrome virus main protease and its complex with an inhibitor, Proc Natl Acad Sci U S A 100 (2003) 13190–13195.
[20] S. Joy, P.S. Nair, R. Hariharan, M.R. Pillai, Detailed comparison of the protein-ligand docking efficiencies of GOLD, a commercial package and ArgusLab, a licensable freeware, Silico Biol. 6 (2006) 601–605.
[21] F. Wu, S. Zhao, B. Yu, Y.M. Chen, W. Wang, Z.G. Song, Y. Hu, Z.W. Tao, J.H. Tian, Y.Y. Pei, M.L. Yuan, Y.L. Zhang, F.H. Dai, Y. Liu, Q.M. Wang, J.J. Zheng, L. Xu, E.C. Holmes, Y.Z. Zhang, A new coronavirus associated with human respiratory disease in China, Nature 579 (2020) 265–269.
[22] E.J. Snijder, P.J. Bredenbeek, J.C. Dobbe, V. Thiel, J. Ziebuhr, L.L. Poon, Y. Guan, M. Rozanov, W.J. Spaan, A.E. Gorbalenya, Unique and conserved features of genome and proteome of SARS-coronavirus, an early split-off from the coronavirus group 2 lineage, J. Mol. Biol. 331 (2003) 991–1004.
[23] C.Y. Chou, H.C. Chang, W.C. Hsu, T.Z. Lin, C.H. Lin, G.G. Chang, Quaternary structure of the severe acute respiratory syndrome (SARS) coronavirus main protease, Biochemistry 43 (2004) 14958–14970.
[24] S.K. Enmozhi, K. Raja, I. Sebastine, J. Joseph, Andrographolide as a potential inhibitor of SARS-CoV-2 main protease: an in silico approach, J. Biomol. Struct. Dyn. (2020) 1–10.
[25] V.S. Nguyen, X.Y. Loh, H. Wijaya, J. Wang, Q. Lin, Y. Lam, W.S. Wong, Y.K. Mok, Specificity and inhibitory mechanism of andrographolide and its analogues as antiasthma agents on NF-kappaB p50, J. Nat. Prod. 78 (2015) 208–217.
[26] J. Wang, X.F. Tan, V.S. Nguyen, P. Yang, J. Zhou, M. Gao, Z. Li, T.K. Lim, Y. He, C.S. Ong, Y. Lay, J. Zhang, G. Zhu, S.L. Lai, D. Ghosh, Y.K. Mok, H.M. Shen, Q. Lin, A quantitative chemical proteomics approach to profile the specific cellular targets of andrographolide, a promising anticancer agent that suppresses tumor metastasis, Mol. Cell. Proteomics 13 (2014) 876–886.
[27] J. Chang, R.M. Zhang, Y. Zhang, Z.B. Chen, Z.M. Zhang, Q. Xu, Y.P. Yang, Y.Y. Long, L.L. Liu, H.Y. Cai, J. Gao, N. Lu, B. Mao, L. Wang, T.Q. Li, [Andrographolide drop-pill in treatment of acute upper respiratory tract infection with external wind-heat syndrome: a multicenter and randomized controlled trial], Zhong Xi Yi Jie He Xue Bao 6 (2008) 1238–1245.
[28] R.A. Burgos, J.L. Hancke, J.C. Bertoglio, V. Aguirre, S. Arriagada, M. Calvo, D.D. Caceres, Efficacy of an Andrographis paniculata composition for the relief of rheumatoid arthritis symptoms: a prospective randomized placebo-controlled trial, Clin. Rheumatol. 28 (2009) 931–946.
[29] C. Calabrese, S.H. Berman, J.G. Babish, X. Ma, L. Shinto, M. Dorr, K. Wells, C.A. Wenner, L.J. Standish, A phase I trial of andrographolide in HIV positive patients and normal volunteers, Phytother Res. 14 (2000) 333–338.
[30] W.J. Sandborn, S.R. Targan, V.S. Byers, D.A. Rutty, H. Mu, X. Zhang, T. Tang, Andrographis paniculata extract (HMPL-004) for active ulcerative colitis, Am. J. Gastroenterol. 108 (2013) 90–98.
[31] S. Gupta, K.P. Mishra, L. Ganju, Broad-spectrum antiviral properties of andrographolide, Arch. Virol. 162 (2017) 611–623.
[32] W. Liao, A.Y.H. Lim, W.S.D. Tan, J. Abisheganaden, W.S.F. Wong, Restoration of HDAC2 and Nrf2 by andrographolide overcomes corticosteroid resistance in chronic obstructive pulmonary disease, Br. J. Pharmacol. (2020).
[33] T. Zhu, W. Zhang, M. Xiao, H. Chen, H. Jin, Protective role of andrographolide in bleomycin-induced pulmonary fibrosis in mice, Int. J. Mol. Sci. 14 (2013) 23581–23596.
[34] H.C. Liao, Y.J. Chou, C.C. Lin, S.H. Liu, A. Oswita, Y.L. Huang, Y.L. Wang, J.L. Syu, C.M. Sun, C.M. Leu, C.H. Lin, S.L. Fu, Andrographolide and its potent derivative exhibit anticancer effects against imatinib-resistant chronic myeloid leukemia cells by downregulating the Bcr-Abl oncoprotein, Biochem. Pharmacol. 163 (2019) 308–320.